

The adsorption and activation of oxygen molecule on nickel clusters doped graphene-based support by DFT

Zhengyang Gao^{a,*}, Ang Li^{a,*}, Xiang Li^a, Xiaoshuo Liu^{a,*}, Chuanzhi Ma^a, Jianmeng Yang^a, Weijie Yang^a, Hao Li^b

^a School of Energy and Power Engineering, North China Electric Power University, Baoding, 071003, China

^b Department of Chemistry and the Institute for Computational Engineering and Sciences, The University of Texas at Austin, 105 E. 24th Street, Stop A5300, Austin, TX, 78712, USA



ARTICLE INFO

Keywords:

Density functional theory
Ni_n nanoclusters
Adsorption characteristics
Catalytic activation
Thermodynamic analysis

ABSTRACT

The catalytic activation of O₂ on nickel nanoclusters doped upon different functionalized graphene substrates (monovacancy as well as one, two and three pyridinic nitrogen decorated) was investigated through the density functional theory calculation. We can observe the adsorption characteristics and the catalytic activation of O₂ on catalysts is related to the support effect of different functionalized graphene supports. The charge of Ni atoms has a good correlation with the adsorption energy of O₂ on Ni_n clusters with different graphene-based support. The electron mainly transferred from the Ni clusters to the O₂, and the graphene-based substrates plays a minor role in the electron transfer process. In addition, the Transition State Scaling are suitable for O₂ dissociation reaction, and Transition State Scaling verify the accuracy of the O₂ dissociation reaction calculation. Furthermore, in accordance with the energy barrier and the thermodynamic analysis of O₂ activation reaction, the Ni₃ clusters catalyst anchored single vacancy graphene decorated with three nitrogen atoms may be the most promising catalyst for O₂ activation reaction. At the same time, this research will cast insight into activation reaction mechanism of O₂ on metal nanoclusters catalysts and lay the foundation for the investigation of metal nanoclusters catalysts for the activation reaction of O₂.

1. Introduction

The fuel cell eliminates the step of converting chemical energy into thermodynamic energy and directly converts it into electrical energy [1,2], which reduced energy loss and improves conversion efficiency. Fuel cell has become a research hotspot with its unique high energy conversion rate, low pollution, no noise and high efficiency. At the anode, the fuel (hydrogen, methanol, etc.) is oxidized, releasing electrons and generating H⁺ ions; at the cathode, oxygen and the H⁺ ions in the electrolyte absorb electrons from the external circuit to form water [3]. However, the rate of reaction of the redox reaction (ORR) is very slow, and the reaction rate must be increased by adding a corresponding catalyst. The Pt/C system is the current mainstream catalyst of ORR [4]. Whereas, high costs [5], slow kinetics of the catalyst [6], and lack of tolerance for fuel crossovers [7] prevent it from continuing to commercialize. Therefore, understanding the ORR reaction mechanism has a great significance for the development of high performance ORR catalysts. The rate of oxygen reduction reaction is very small, which indicated that increasing the reaction rate of the cathode is

the top priority to increase the redox reaction rate. The oxygen catalyzed dissociation is a significant procedure and a standard to indicate the activation capacity of the ORR reaction [8]. So the paper focuses on high activity catalysts of O₂ dissociation process.

Graphene is a promising metal-free ORR catalyst with its unique two-dimensional hexagonal honeycomb structure, superior thermal conductivity, superior electrical conductivity and huge specific surface area [9–12]. Yan [13] et al. compared the O₂ activation reaction of graphene and nitrogen doped graphene, and found that nitrogen doped graphene can strengthen the adsorption energy of O₂ and decrease the energy barrier of O₂. Li [14] et al. investigated the effect of sulfur-doped graphene on oxygen activation reaction. It is found that S-doped graphene inhibits oxygen adsorption and significantly decreases dissociation barriers of the O₂ molecules. Tang [15] et al. calculated the oxygen activation reaction on different BN clusters and found that the energy barrier of O₂ on the N-terminated triangular BN (t-BN) cluster is less than O₂ on the t-BN with B edge and quadrangular BN (q-BN).

Nowadays, non-precious transition metal carbon catalysts has been also studied as a catalyst for ORR. Gao [16] et al. investigated the

* Corresponding authors.

E-mail addresses: gaozhyang@163.com (Z. Gao), hualioang@163.com (A. Li), liuxiaoshuo@ncepu.edu.cn (X. Liu).

<https://doi.org/10.1016/j.mcat.2019.110547>

Received 24 April 2019; Received in revised form 31 July 2019; Accepted 1 August 2019

Available online 08 August 2019

2468-8231/ © 2019 Published by Elsevier B.V.

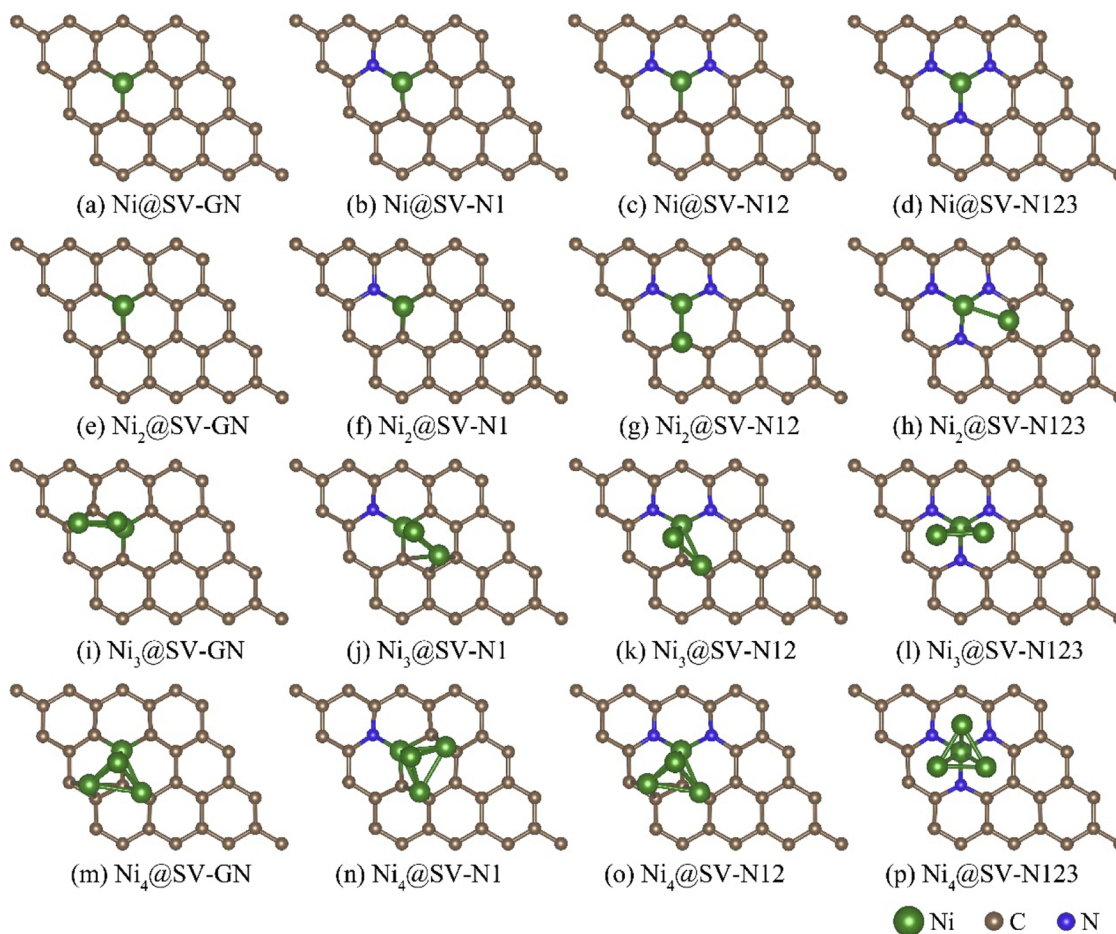


Fig. 1. The geometry structures (the top view) of $Ni_n@SV-GS$ catalysts.

Table 1

The structural and energetic parameters for the most stable adsorbed geometries of $Ni_n@SV-GS$ catalysts.

$Ni_n@SV-GS$	$E_b(\text{eV})^a$	$h(\text{\AA})^b$	$\Delta q(\text{e})^c$	$d_{\text{Ni-Ni}}(\text{\AA})^d$	$E_c(\text{eV})^e$	$E_{c/GM}(\text{eV})^f$
Ni@SV-GN	-6.65(-6.69 [40])	1.28	+0.50	/	-4.44	-6.69
Ni@SV-N1	-5.34(-5.36 [40])	1.27	+0.60	/	-4.44	-5.36
Ni@SV-N12	-5.05(-5.00 [40])	1.40	+0.70	/	-4.44	-5.00
Ni@SV-N123	-4.52(-5.09 [45])	1.38	+0.77	/	-4.44	-4.32
$Ni_2@SV-GN$	-8.04(-8.05 [40])	1.20	+0.91	2.40(2.34 [44])	-1.42	-5.44
$Ni_2@SV-N1$	-5.84(-5.84 [40])	1.24	+1.02	2.51	-1.42	-4.34
$Ni_2@SV-N12$	-4.88(-4.88 [40])	1.42	+0.71	2.22	-1.42	-3.86
$Ni_2@SV-N123$	-3.66(-4.44 [45])	1.40	+0.76	2.32	-1.42	-3.25
$Ni_3@SV-GN$	-6.62(-6.63 [40])	1.41	+0.55	2.25(2.33 [44])	-1.84	-4.05
$Ni_3@SV-N1$	-5.13(-5.17 [40])	1.36	+0.64	2.27	-1.84	-3.56
$Ni_3@SV-N12$	-5.17(-5.17 [40])	1.45	+0.71	2.26	-1.84	-3.56
$Ni_3@SV-N123$	-4.22(-5.22 [45])	1.48	+0.58	2.24	-1.84	-3.25
$Ni_4@SV-GN$	-6.95(-6.98 [40])	1.46	+0.79	2.35(2.36 [44])	-2.15	-3.89
$Ni_4@SV-N1$	-5.69(-5.75 [40])	1.51	+0.87	2.34	-2.15	-3.58
$Ni_4@SV-N12$	-5.45(-5.56 [40])	1.44	+0.92	2.35	-2.15	-3.54
$Ni_4@SV-N123$	-4.44(-5.74 [45])	1.48	+0.63	2.29	-2.15	-3.25

^a The binding energies of $Ni_n@SV-GS$ catalysts, calculated from Eq. (1).

^b The changing altitude of Ni clusters over substances. (The changing altitude of the Ni clusters was defined as the vertical distance from the center of bottom Ni atom to the substrates).

^c After geometry optimization, the electron gain and loss of Ni clusters. ("+" was on behalf of electronic outflow and "-" means electronic inflow).

^d After geometry optimization, the average Ni-Ni bond length of each Ni clusters.

^e The cohesive energy of gas-phase, calculated from Eq. (6).

^f The cohesive energy of graphene-based Ni clusters, calculated from Eq. (7).

oxygen activation reaction on Fe/graphene-based substrates, and found that iron atom with single vacancy graphene anchored three N atoms is a promising catalyst for oxygen activation reaction. Zhang [17] et al. investigated the adsorption of oxygen on the Au/graphene catalyst with

an applied electric field, and found that the adsorption of oxygen on the catalyst is enhanced and the oxygen-oxygen bond is also elongated under a negative power plant. Liu [18] et al. have shown the oxygen dissociation reaction at the Pt/graphene-based substrates and Pt₄

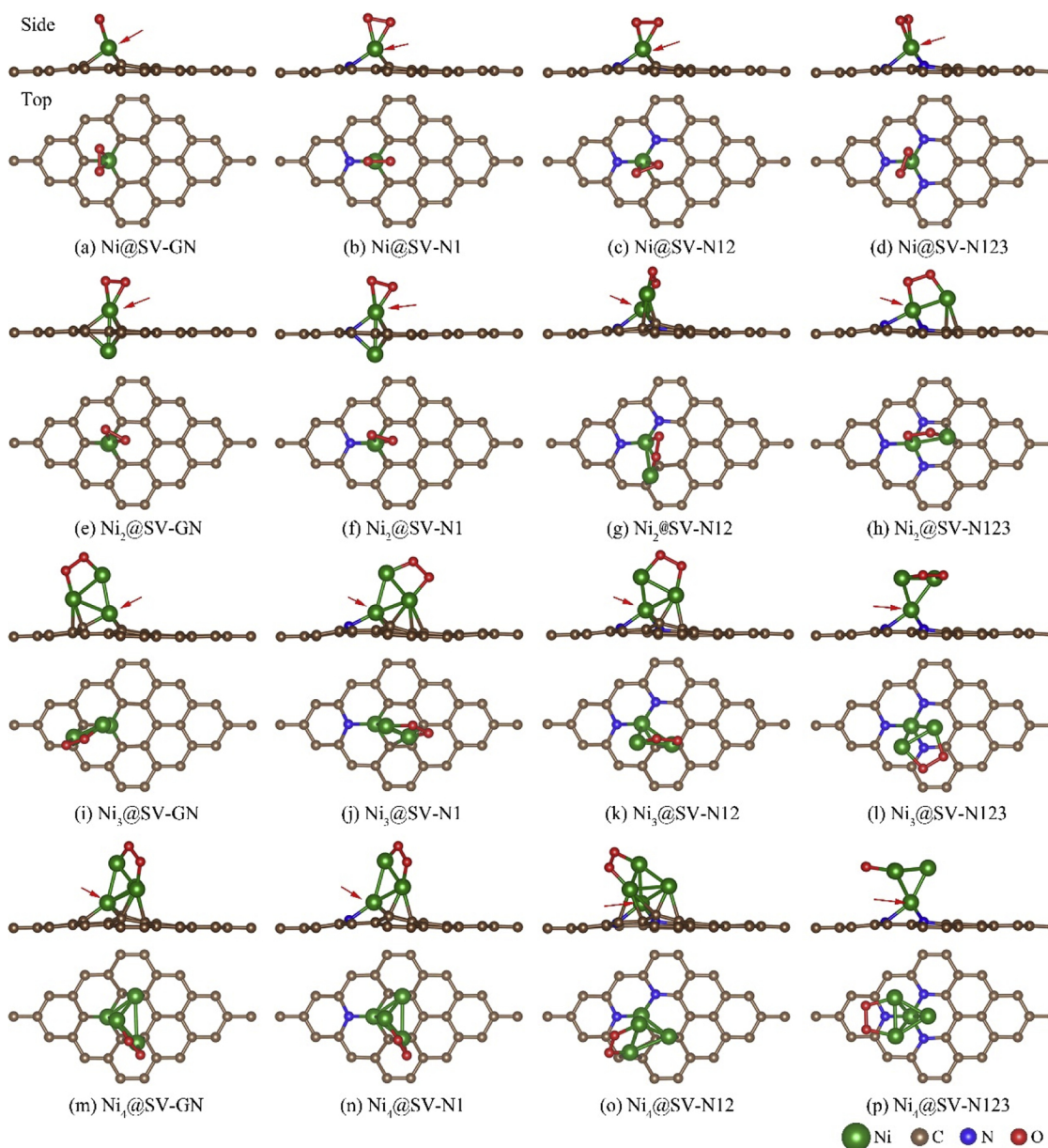


Fig. 2. The optimized configuration (the top view) of oxygen adsorbed on the $Ni_n@SV-GS$ catalysts.

clusters/graphene-based substrates, and it is found that the loss electrons of Pt/ Pt_4 clusters have a great effect on the energy barrier of O_2 dissociation reaction and the energy barriers of O_2 dissociation reaction on Pt_4/GS are much smaller than O_2 dissociation reaction on Pt/GS. However, the Pt is a noble metal, which leads to high manufacturing costs for this catalyst. Therefore, finding an inexpensive transition metal to replace expensive Pt is the focus of this paper. Ni atom are the same group as Pt atoms, chemically similar, and Ni is a non-noble metal atom. Previous studies have investigated the activation of molecules in Ni or related Ni-systems. Millet [19] et al. have study the activation of CO_2 on the Ni Single Atom Catalysts, and found that Ni single atom catalysts promotes the activation of CO_2 . Fiedler [20] et al. studied the activation of O_2 on the Mn, Co, Ni metal centers and enzymatic environments. But the oxygen activation reaction on Ni clusters has never studied. So Ni clusters/graphene-based substrates are used as catalysts to study the oxygen dissociation reaction. In addition, previous researches have been discovered that graphene with single absence increases itself stability [21,22]. The N-doped graphene increases the reactivity by creating local active sites in the graphite lattice [23,24].

So the graphene with single vacancy and doping nitrogen are chosen as the functionalized graphene substrates, and the Ni_n clusters doped the functionalized graphene substrates are denoted as $Ni_n@SV-GN$, $Ni_n@SV-N1$, $Ni_n@SV-N12$ and $Ni_n@SV-N123$, respectively.

In this work, we investigated the activation of oxygen molecule on Ni_n cluster/functionalized graphene substrates ($Ni_n@SV-GS$, $n = 1, 2, 3$ and 4) by performing density functional theory (DFT). Firstly, the optimized configurations of $Ni_n@SV-GS$ catalyst and the optimal adsorption configurations of O_2 molecule on $Ni_n@SV-GS$ catalysts were optimized. Secondly, the correlation between the adsorption energy of O_2 and the charge of Ni atom was analyzed, and the electron transfer mechanism of O_2 on $Ni_n@SV-GS$ was proposed to interpret who gets the electron and who loses the electron. Thirdly, the DOS analysis and magnetic properties analysis were performed to investigate the interaction between the catalyst and the oxygen molecule. Then, the energy barriers of O_2 activation reaction was proposed to analyze the catalytic performance of $Ni_n@SV-GS$ catalysts on O_2 dissociation. Finally, the thermodynamic analysis have been calculated to analyze the influence of temperature about O_2 activation reaction. This work can provide a

Table 2

The structural and electronic parameters for O₂ adsorbed on Ni_n@SV-GS catalyst.

Ni _n @SV-GS	$E_{\text{ads}}(\text{eV})^a$	$d_{\text{O-O}}(\text{\AA})^b$	$d_{\text{Ni-Ni}}(\text{\AA})^c$	$\Delta h(\text{\AA})^d$	$q_1(\text{e})^e$
Ni@SV-GN	-1.62	1.35	\	+0.15	9.22
Ni@SV-N1	-1.90	1.37	\	+0.09	9.11
Ni@SV-N12	-2.16	1.41	\	-0.05	8.99
Ni@SV-N123	-2.48	1.37	\	+0.09	9.00
Ni ₂ @SV-GN	-1.46	1.34	2.44	+0.13	9.21
Ni ₂ @SV-N1	-2.19	1.35	2.53	+0.04	9.15
Ni ₂ @SV-N12	-2.71	1.43	2.23	-0.01	9.15
Ni ₂ @SV-N123	-3.16	1.42	2.23	-0.03	9.12
Ni ₃ @SV-GN	-2.55	1.41	2.38	-0.03	9.60
Ni ₃ @SV-N1	-2.52	1.41	2.32	-0.04	9.55
Ni ₃ @SV-N12	-2.60	1.43	2.34	-0.01	9.59
Ni ₃ @SV-N123	-2.01	1.42	2.32	+0.00	9.40
Ni ₄ @SV-GN	-2.73	1.41	2.45	+0.04	9.57
Ni ₄ @SV-N1	-2.55	1.43	2.38	-0.02	9.50
Ni ₄ @SV-N12	-2.37	1.42	2.39	-0.00	9.46
Ni ₄ @SV-N123	-2.44	1.43	2.33	-0.01	9.43

^a The adsorption energy of O₂ on different nickel nanocluster catalysts, calculated from Eq. (2).

^b After O₂ adsorbed on nickel nanocluster catalysts, the bond length of oxygen molecules.

^c After O₂ adsorbed on nickel nanocluster catalysts, the average Ni-Ni bond length of each Ni clusters.

^d The variation of adsorption height of Ni_n clusters. (The variation of adsorption height of Ni_n clusters was defined as the change in height of Ni_n clusters after oxygen adsorption and before oxygen adsorption).

^e After O₂ adsorbed on nickel nanocluster catalysts, the charge of Ni atom anchored on the vacancy of graphene substrate.

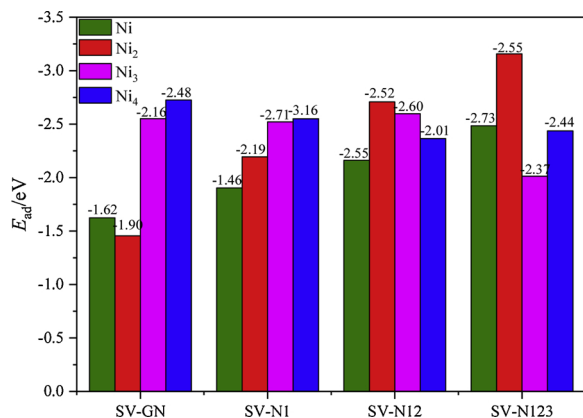


Fig. 3. The histogram of O₂ adsorption energies over different Ni_n@SV-GScatalysts.

new idea on develop the efficient catalysts about O₂ activation.

2. Method

Vienna ab initio simulation package software (VASP 5.4.4) was used to perform DFT calculations, with the consideration of spin-polarized effect [25–27]. The method of Perdew-Burke-Ernzerhof (PBE) [28,29] was selected for calculations, combined with the potential of the projector augmented wave (PAW), to increase the accuracy of the calculation. In addition, the Perdew-Burke-Ernzerhof (PBE) could be well illustrated the exchange-correlation interactions of electron [30]. Similar to previous calculation results [31–34], a 4 × 4 single layer graphene was selected as the support, and this support is a periodic boundary model. The distance about the two adjacent monolayers was set to 15 Å, which was prevented mutual influence about mirror images. Moreover, the lattice parameters of graphene was calculated about 2.48 Å, which is the same as the earlier theoretical and experimental

studies [35,36].

Taking into account computing resource and referring to our previous research [37–42], the cut off energy for all geometric optimization calculation was set about 500 eV. The Gaussian smearing width was set at 0.05 eV level to characterize the electronic occupation. All atoms were achieved fully relax on structural optimization works, and the force threshold of atoms cannot exceed 0.02 eV/Å, with a 7 × 7 × 1 Γ-centered k-point grid. Denser k-point grid (15 × 15 × 1) was used to calculate the self-consistent field, to further calculate the total energy and the electronic characteristic of the system. For the structure optimization and the electronic self-consistent iteration calculation, the convergence precision criterion was taken to be 10⁻⁵ eV. In addition, the ISPIN was set about 2, which indicated that the calculation was considered spin polarization.

The climbing images nudged elastic band (CI-NEB) was used to hunt for the transition states, which insert eight images between the original structure and eventual structure. The vibration frequency was carried out with limited modification of ± 0.02 Å in distance changes, which was utilized to verify accuracy of each transition state structure [16]. In addition, in order to obtain the accurate system energy, the zero point correction is calculated. The most stable optimized structure has no virtual frequency, but there is only one virtual frequency for the transition state of the reaction.

The binding energy (E_b) of Ni_n@SV-GS ($n = 1-4$) catalysts could be acquired from Eq. (1).

$$E_b = E_{\text{sur+Ni}_n} - E_{\text{sur}} - E_{\text{Ni}_n} \quad (1)$$

Where $E_{\text{sur+Ni}_n}$, E_{sur} and E_{Ni_n} represent the ground-state energy of Ni_n cluster catalysts, graphene-based supports and nickel clusters, respectively.

The adsorption energy (E_{ads}) of O₂ on Ni_n@SV-GS ($n = 1-4$) catalysts were computed to characterize the adsorption strength about the adsorbent and the adsorbate, which were computed as following Eq. (2).

$$E_{\text{ads}} = E_{\text{tot}} - E_{\text{sur+Ni}_n} - G_{\text{O}_2(\text{g})} \quad (2)$$

Where E_{tot} , $E_{\text{sur+Ni}_n}$ and $G_{\text{O}_2(\text{g})}$ represent the ground-state energy of the total adsorption system, the ground-state energy Ni cluster catalysts and the Gibbs free energy of oxygen molecule, respectively. We found from the Eq. (2), the farther the values of E_{ads} from zero, the stronger adsorption strength of catalysts.

The Gibbs free energy of oxygen molecule were calculated according to Eq. (3).

$$G_{\text{O}_2(\text{g})} = 2G_{\text{H}_2\text{O}(\text{l})} - 2G_{\text{H}_2(\text{g})} + 4 \times 1.23\text{eV} \quad (3)$$

Where $G_{\text{H}_2\text{O}(\text{l})}$ and $G_{\text{H}_2(\text{g})}$ represent the Gibbs free energy of water and hydrogen molecule, respectively.

The Gibbs free energy of gases and solid subjects can be calculated from the Eqs. (4) and (5):

$$G_{\text{gas}}(T) = E_{\text{ele}} + \text{ZPE} + RT - TS \quad (4)$$

$$G_{\text{solid}}(T) = E_{\text{ele}} + \text{ZPE} - TS \quad (5)$$

Where E_{ele} and ZPE mean the energy of the whole system and the zero correction energy; S represents the entropy of the system. The ZPE and S are obtained by the frequency calculation.

The cohesive energy for both gas-phase (E_C) and graphene-based Ni clusters ($E_{C/\text{GM}}$) were calculated according to Eqs. (6) and (7).

$$E_C = (E_{\text{Ni}_n} - nE_{\text{Ni}})/n \quad (6)$$

$$E_{C/\text{GM}} = (E_{\text{Ni}_n/\text{GM}} - E_{\text{GM}} - nE_{\text{Ni}})/n \quad (7)$$

Where E_{Ni_n} , E_{Ni} , $E_{\text{Ni}_n/\text{GM}}$, E_{GM} and n represent the energy of Ni cluster, Ni atom, Ni cluster catalysts, graphene-based supports and the number of Ni atoms in Ni cluster, respectively.

The energy barrier (E_{bar}), the activation energy (E_a) and the reaction heat (ΔE) were computed to describe the catalytic activity of Ni_n cluster

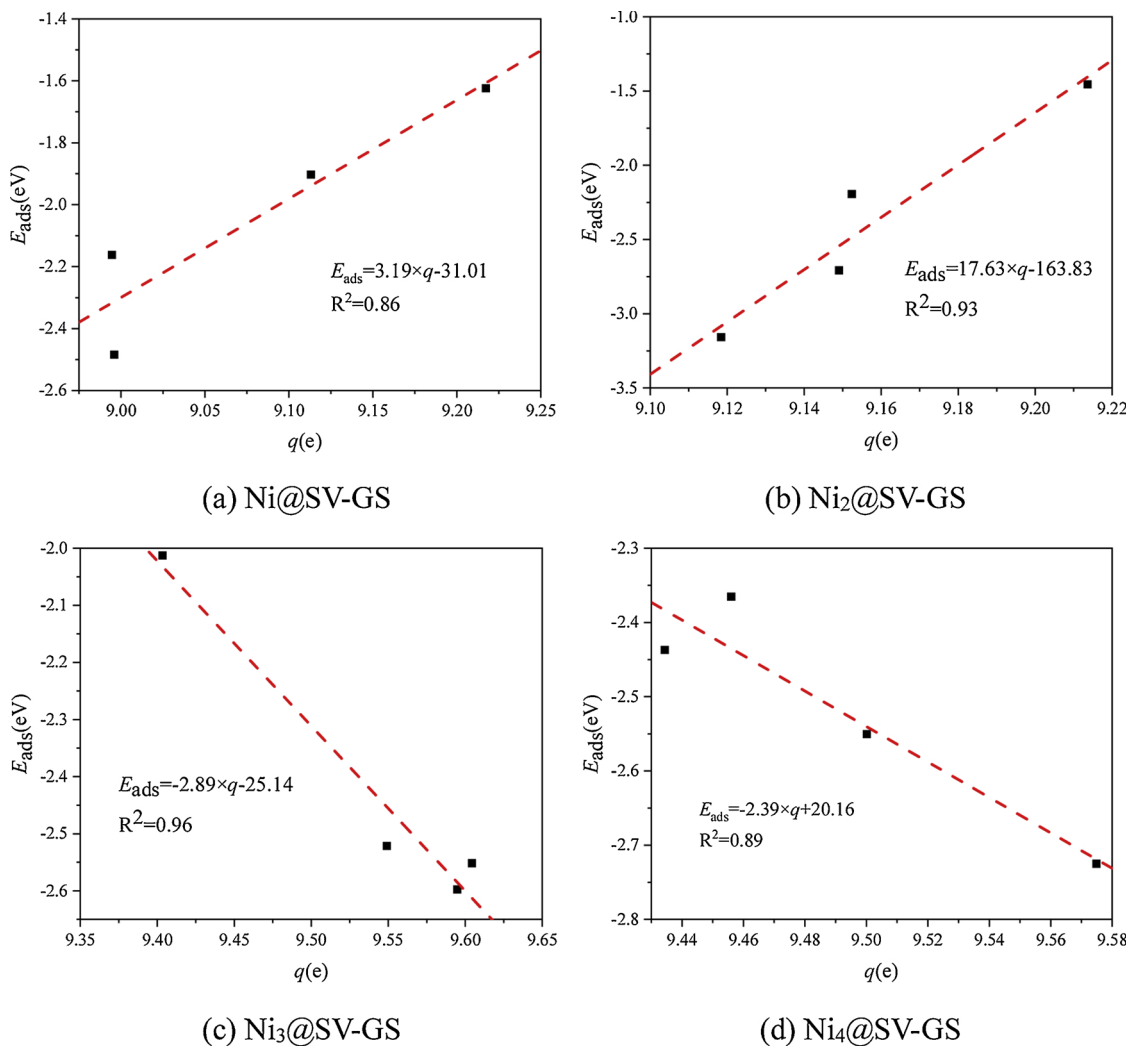


Fig. 4. The linear relationship and the correlation coefficient between the adsorption energies of O₂ on the Ni_n@SV-GS as well as the amount of charge carried by the nickel clusters.

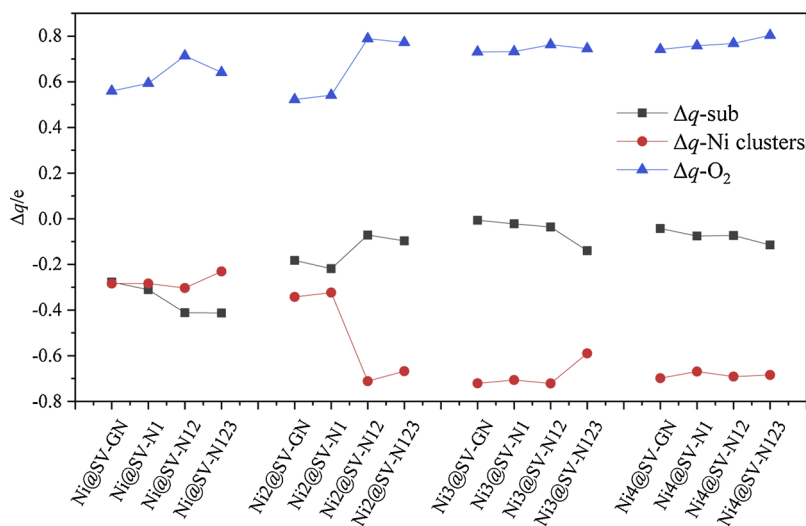


Fig. 5. The line chart of the electron transfer of O₂, Ni clusters and graphene-based substrates (Δq -O₂, Δq -Ni Cluster and Δq -sub represent the electron transfer of O₂, Ni clusters and graphene-based substrates, respectively).

Table 3
The magnetic moment of O₂ on the Ni_n@SV-GS catalysts.

M(μB)	sv	sv-n	sv-n2	sv-n3
ni	1.61	-0.49	0.00	1.00
ni2	1.08	-0.80	0.00	0.80
ni3	2.00	1.00	2.00	5.00
ni4	2.00	1.02	2.48	5.00

catalyst, which were calculated according to Eqs. (8) and (9).

$$E_{\text{bar}} = E_a = E_{\text{TS}} - E_{\text{IS}} \quad (8)$$

$$\Delta E = E_{\text{FS}} - E_{\text{IS}} \quad (9)$$

Where E_{IS} , E_{TS} and E_{FS} represent the initial states energy, transition states energy and the final states energy, respectively.

Furthermore, in order to get accurate values of E_b , E_{ads} and E_{bar} , the zero point energy correction is performed [43].

3. Result and discussion

3.1. Research model

According to the first part of this paper, sixteen kinds of functionalized graphene substrates with single vacancies and nitrogen atoms decorated were selected as the catalysts construction, and the optimized configuration of catalysts are shown in Fig. 1. The structural and energetic parameters for the most stable adsorbed geometries of Ni_n@SV-GS catalyst are shown in Table 1. According to the Fig. 1(a) and (e), the most stable geometric structures of Ni@SV-GN and Ni₂@SV-GN are similar. In fact, they are totally different. Fig. 1 is a top view, and we can find that the geometric structure of Ni₂@SV-GN is two Ni atoms locating on the upper and lower sides of the graphene, as shown in Fig. S1. Similarly, the same is true for Fig. 1(b) and (f).

The catalysts of Ni cluster on the graphene with single vacancy decorated nitrogen atoms have been widely studied in the previous researches. Xu [44] et al. studied Ni_n clusters on the single vacancy graphene (Ni_n@SV-GN), and the mean length value of Ni-Ni bond of each nickel clusters in this paper is very close to that calculated by Xu. Gao [40] et al. investigated Ni_n clusters on the single vacancy graphene decorated nitrogen atoms (Ni_n@SV-GS), and the E_b calculated by Gao is

much close to the calculation results, which proves the correctness of this calculation. Zhou [45] et al. calculated the E_b of Ni_n@SV-N123. But the values vary greatly to our results (almost 0.77~1.30 eV difference), which may be related to the differences in calculation software and parameter selection Ni_n@SV-GS Ni_n@SV-GS. The average length of carbon-carbon bond is 1.42 Å, which is similar to the previous calculation results. ($d_{\text{C-C}} = 1.42 \text{ \AA}$) [46].

In addition, in order to verify the stability of the Ni metal clusters, the cohesive energy for both gas-phase (E_c) and graphene-based Ni clusters ($E_{c/GM}$) were calculated, as shown in Table 1. It can be found that the cohesive energy of graphene-based Ni clusters ($E_{c/GM}$) is greater than the cohesive energy of gas-phase (E_c). That is to say, the Ni atom is more willing to bind to the Ni cluster in which it is located, rather than the Ni cluster around it. It is indicated that the Ni_n@SV-GS catalysts are very stable and the Ni atoms of the Ni_n@SV-GS catalysts do not cohere together. This verifies the accuracy of the calculated catalyst configuration. So the optimized catalyst models and the calculated structural parameters are accurate.

3.2. Adsorption of O₂ molecule on Ni_n@SV-GS

There are mainly two types of adsorption configurations for oxygen adsorption, side-on and end-on. The side-on is the O–O bonds parallel to the graphene-based substrates or the Ni-Ni bonds, the end-on is the O–O bonds vertical to the graphene-based substrates and only one oxygen atom correcting to the Ni metal atoms. The side-on and the end-on adsorption configuration of Ni_n@SV-GS ($n = 1, 2, 3$ and 4) adsorbing oxygen molecule are calculated. We screen out the optimal adsorption configuration, as shown in Fig. 2. It can be found from Fig. 2 that the optimal adsorption configuration of oxygen is the same, which prefers the O–O bonds paralleling to the graphene-based substrates or the Ni-Ni bonds (the side-on configuration). The structural and energetic parameters for the most stable adsorbed geometries of O₂ on Ni_n@SV-GS catalysts are listed in Table 2.

The sixteen catalyst configurations listed in Fig. 1 were discussed to analyze the support effects. The structural and energetic parameters were used to analyze the support effects, and the histogram of the adsorption energy of these 16 configurations for oxygen is plotted in Fig. 3. The adsorption energies for oxygen molecules on different graphene-based substrates are significantly different from Fig. 3, while there are no obvious relationship between those E_{ads} . Although the

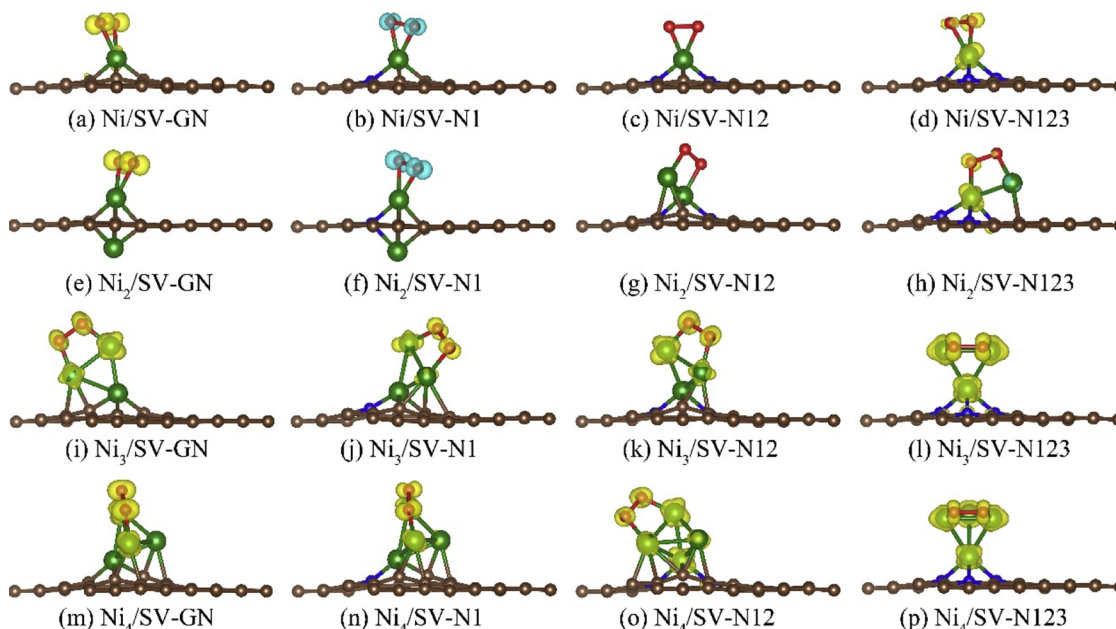


Fig. 6. The spin density of the O₂ adsorbed on the Ni_n@SV-GS. (The contour lines in plots are drawn at 0.02e/Å³ intervals).

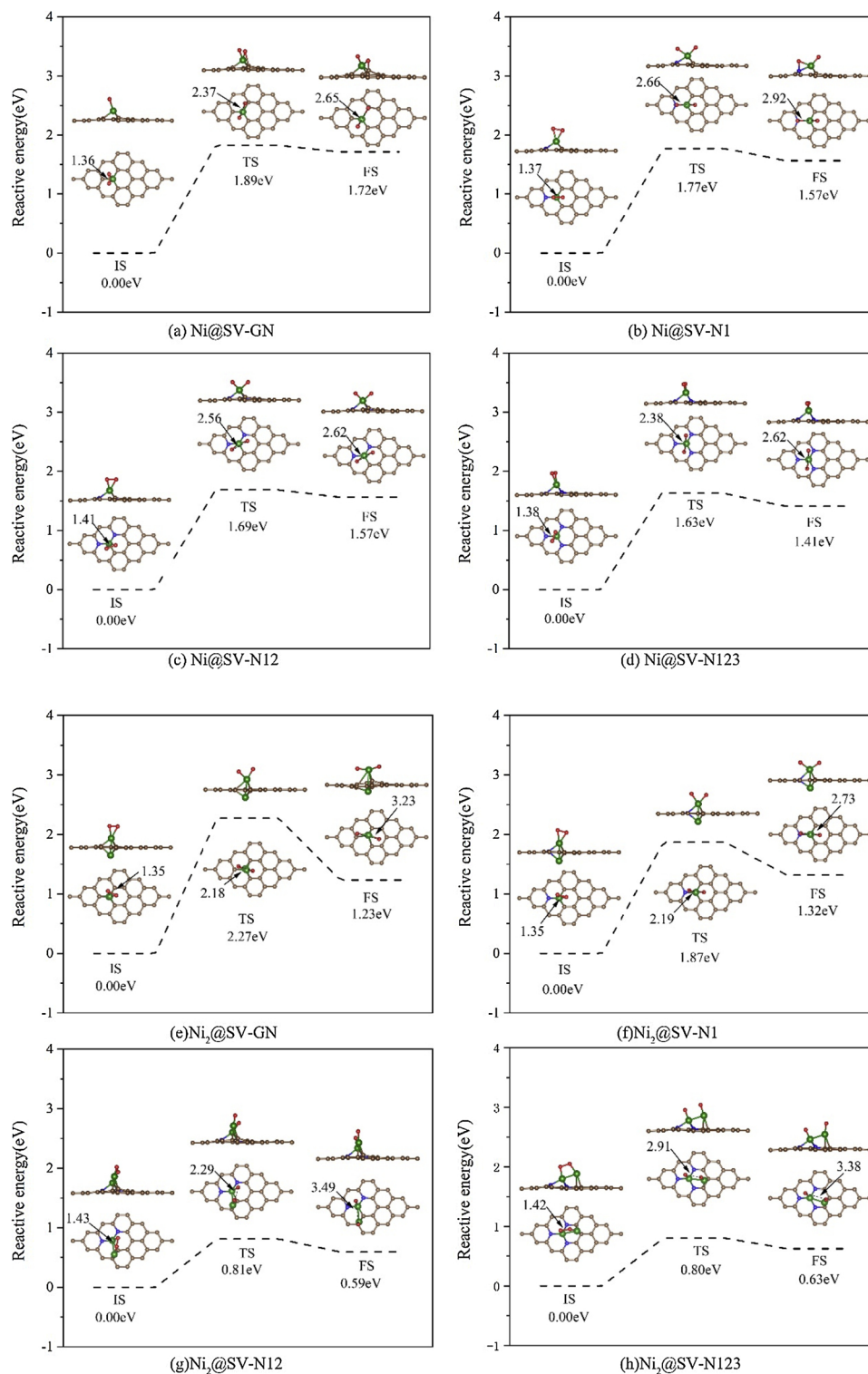


Fig. 7. Schematic energy profiles of the oxygen dissociation reaction..

adsorption energy is not very regular, it still suggests that the adsorption energy of oxygen for different graphene-based substrates is different, thus verifying the support effect. Therefore, this paper will further study the reason why the adsorption energy is so irregular.

In the research of Liu [18], the correlation between the E_{ads} of O_2 and the charge of Pt atom was discussed. They found that there is an obvious positive correlation between the E_{ads} of O_2 and the charge of platinum atom, and the charge of platinum atoms is a main influencing factor for the E_{ads} of O_2 . So the relevance between the E_{ads} of O_2 on the

graphene-based supports and the charge of Ni atom anchored on the vacancy of graphene substrate (Ni atom pointed by red arrow in Fig. 2) was discussed, and the intersecting line and R^2 of the related line are plotted in Fig. 4. It can be found that a strong linear relationship between the E_{ads} of O_2 on $\text{Ni}_n\text{@SV-GS}$ catalysts and the charge of Ni atom, and R^2 are 0.86, 0.93, 0.96 and 0.89 respectively. It is indicated that the charge of Ni atom anchored on the vacancy of graphene substrate seems to be a descriptor of the adsorption energy of O_2 . In summary, it explains why the adsorption energy is so irregular.

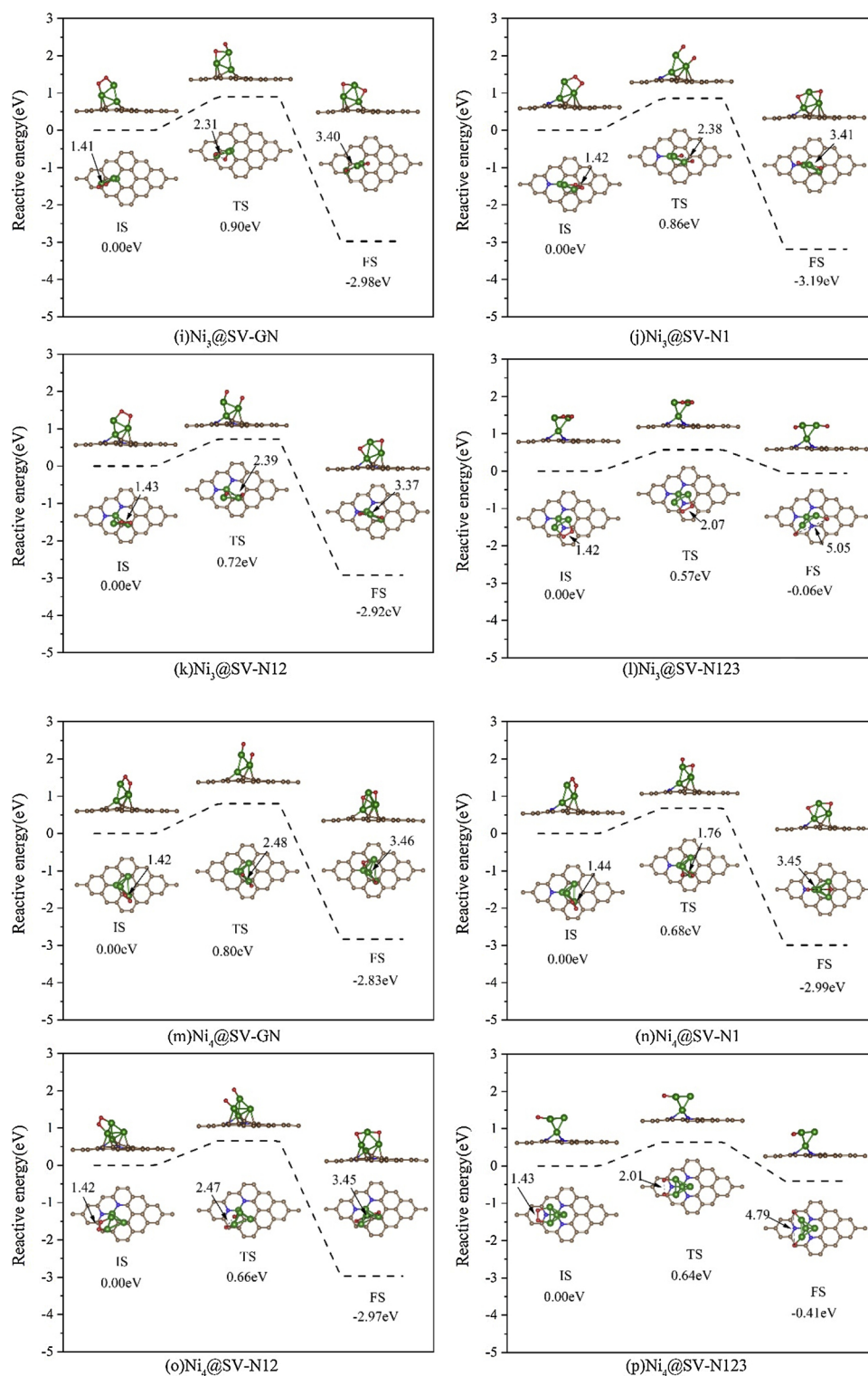


Fig. 7. (continued)

In order to find the mechanism of oxygen adsorption on catalysts, the Bader charge analysis is performed. So the electron transfer of O₂, Ni clusters and graphene-based substrates before and after oxygen adsorption were calculated, and the detailed data are provided in Table S1. A line chart of the charge transfer situation for each part of those sixteen systems are plotted in Fig. 5. It can be found that graphene-based substrates always transport electrons outward but oxygen molecule receive electrons inward all the time, from the Fig. 5. When O₂ was adsorbed on Ni@SV-GS, O₂ played the role of electrons acceptor, and Ni

atoms as well as the functional graphene supports played the role of electron donor. However, the electron loss of the functional graphene is an order of magnitude less than Ni clusters, when O₂ adsorbed on Ni_n@SV-GS ($n = 2, 3$ and 4). Particularly, the number of electron loss of graphene-based substrates on Ni₃@SV-GN is 0.007e, which only accounted for less than 1% of the electron loss of Ni clusters (0.721e). So the electron loss of graphene-based substrates can be ignored and Ni clusters act as the electron donor. It is obvious that the electron mainly transfer from the Ni clusters to the O₂, and the graphene-based

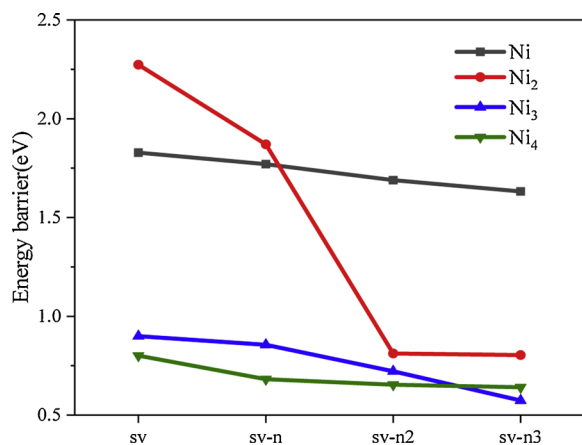


Fig. 8. The energy barrier of oxygen dissociation reaction.

substrates plays a minor role in the electron transfer process.

3.3. DOS and magnetic properties analysis

In order to further investigate the interaction between the catalyst and the oxygen molecule, the DOS analysis and magnetic properties analysis were performed. The partial density of states (PDOS) can provide an electronic state in an orbit of an atom in the system. So the PDOS of oxygen molecule adsorbed on catalysts was drawn in Fig. S2, and the magnetic moment of the O₂ on catalysts was calculated, as shown in Table 3.

From the Fig. S2, the p orbit of O atom and the d orbit of Ni atom in the total adsorption system were drawn, and the p orbit of O atom before and after adsorption were drawn too. It can be found that the p orbit sharp peaks of O atom is -0.23 eV before the oxygen adsorbed on the catalyst. And the p state of O atom is shifted down to a low energy level when oxygen is adsorbed on the catalyst. It is indicated that oxygen interacts with the catalyst when oxygen is adsorbed on the catalyst. This is consistent with the results of the above Bader charge analysis.

According to the magnetic moment of each catalytic system (Table 3), it can be found that the magnetic moments of Ni/SV-N1 and Ni₂/SV-N1 are negative, and the magnetic moments of Ni/SV-N12 and Ni₂/SV-N12 are zero, except that the others are positive. In order to verify the accuracy of the calculated magnetic moment, the spin density

of the O₂ adsorbed on the Ni_n/SV-GS is plotted, as shown in Fig. 6. From the Fig. 6, the yellow represents spin up and the cyan represents spin down. The O₂ of Ni/SV-N1 and Ni₂/SV-N1 are surrounded by cyan color which show the oxygen molecule is spin down, thus proves that the magnetic moment is negative. The O₂ of Ni/SV-N12 and Ni₂/SV-N12 are neither surrounded by yellow nor surrounded by cyan which show the oxygen molecule have no spin, thus proves that the magnetic moment is zero. Except that the others are surrounded by yellow color which show the oxygen molecule is spin up, thus proves that the magnetic moment is positive. In addition, the spin up and spin down of PDOS is same from Fig. S2 (c) and (g), which indicated that the system of O₂ on Ni/SV-N12 and Ni₂/SV-N12 have no spin. Thus proving the accuracy of the calculated magnetic moment. According to the Bader charge analysis and DOS analysis, when the Ni cluster is doped on the graphene to form a catalyst, the Ni cluster will gain electrons from the graphene. The d orbital of Ni atom will gain electrons. Oxygen molecule has the half-filled 2π* orbitals, which is an antibonding molecular orbital. When oxygen is adsorbed on the Ni_n@SV-GS catalyst, the electron of Ni cluster gained from the graphene will transfer to oxygen molecule, which will occupy the antibonding molecular orbital of oxygen molecule. It will cause the bond length of oxygen to be lengthened. The bond lengths of oxygen are listed in Table S1, which ranges from 1.35 Å to 1.43 Å. Comparing with the free oxygen (1.21 Å), the bond length of oxygen is lengthened. It is indicated that O₂ is already activated. In addition, the Ni_n@SV-GS catalysts has a certain catalytic effect on the activation of oxygen molecule.

3.4. Catalytic activation of O₂ activation

In order to research the catalytic activity of these sixteen catalysts (Ni_n@SV-GS) for oxygen activation, we applied the CI-NEB method to search for transition states in each reaction path of oxygen catalytic activity. The optimal adsorption configuration calculated in Section 3.2 is taken as the initial configuration, and the oxygen-oxygen bond of the initial configuration is elongated and optimized to obtain the final configuration. By performing CI-NEB calculations between the initial configuration and the final configuration, we can derive the transition states and the process of the entire dissociation reaction. The geometry and parameters of each dissociation process were plotted in Fig. 7. The line chart of oxygen reaction energy barrier is plotted in Fig. 8, and it can be found that the reaction barriers of oxygen on Ni_n@SV-GS decrease as the amount of the number of nitrogen doping increases.

From Fig. 7, the O atom is bond with two Ni atoms on the final states of Ni_n@SV-GN, Ni_n@SV-N1 and Ni_n@SV-N12 (n = 3 and 4), which

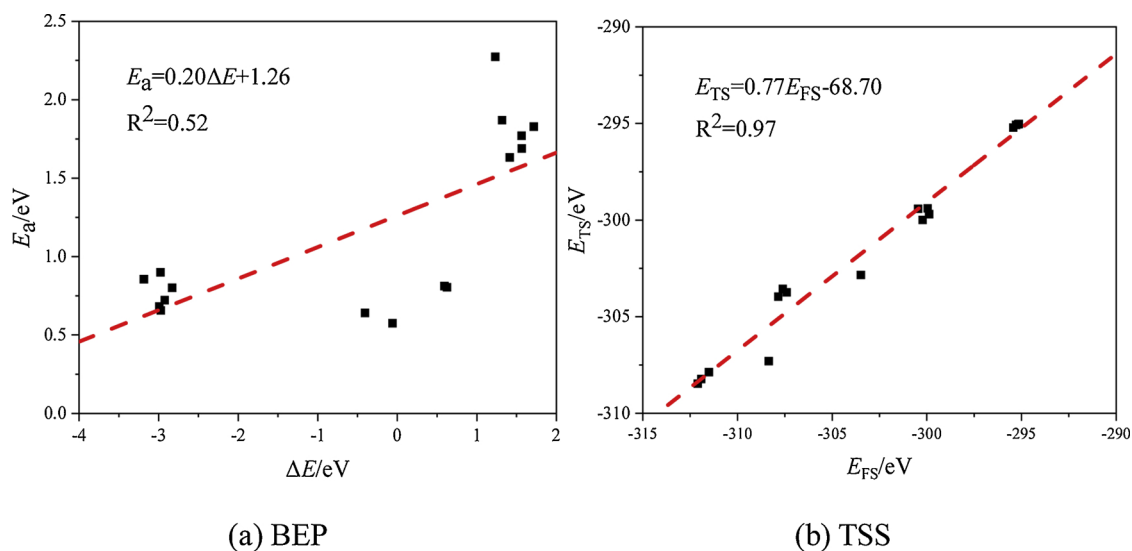


Fig. 9. BEP and TSS of oxygen activation on Ni_n@SV-GS catalysts.

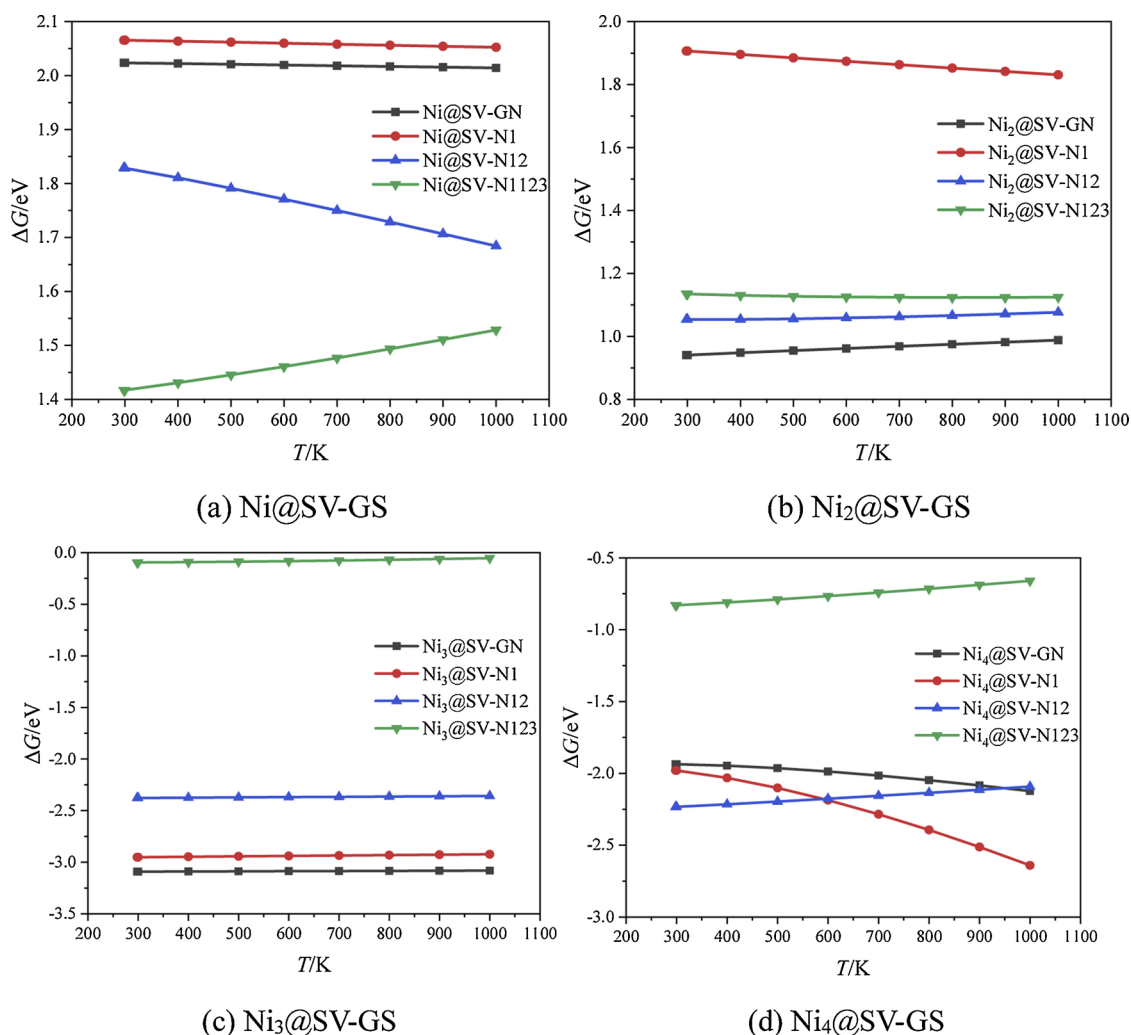


Fig. 10. The Gibbs free energy of O₂ activation reaction on Ni_n@SV-GS at different reaction temperatures.

is indicated that the O atom is difficult to remove in the oxidation reaction and Ni_n@SV-GN, Ni_n@SV-N1 and Ni_n@SV-N12 ($n = 3$ and 4) are not a good catalyst for O₂ activation reaction. From Fig. 8, the energy barriers of O₂ dissociation reaction are 1.63–2.27 eV on Ni@SV-GS, Ni₂@SV-GN and Ni₂@SV-N1, which are much larger than the energy barrier of O₂ on single atom catalysts (1.12 eV [16] of Fe@SV-N123 and 1.09 eV [18] of Pt@SV-N123). It is indicated that the Ni@SV-GS, Ni₂@SV-GN and Ni₂@SV-N1 are not a good catalyst for O₂ activation reaction. In summary, the energy barriers of O₂ dissociation reaction about Ni₂@SV-N12, Ni₂@SV-N123, Ni₃@SV-N123 and Ni₄@SV-N123 are 0.81 eV, 0.80 eV, 0.57 eV and 0.64 eV, respectively, which are less than our previous calculation of the energy barrier for O₂ on single iron atom catalysts (the minimum energy barrier is 1.12 eV [16]). It is indicated that Ni₂@SV-N12, Ni₂@SV-N123, Ni₃@SV-N123 and Ni₄@SV-N123 may become potential catalysts for oxygen activation with its good adsorption configuration and low reaction energy barrier.

To further analyze the activation energy (E_a) and the reaction heat (ΔE), the Brønsted-Evans-Polanyi (BEP) and Transition States Scaling (TSS) relations are proposed. The BEP is an empirical formula, which was first proposed by Brønsted, Evans and Polanyi [47,48]. The equation is shown in Eq. (10), and it shows that the activation energy (E_a) of an elementary reaction has a great linear relationship with the reaction heat (ΔE). Pallassana [49] et al first applied the BEP relationship on heterogeneous catalysis, and found that the E_a and the ΔE of ethylene on different Pd surfaces show a good linear relationship. Recently, with the intention of finding the relationship between transition state energy

(E_{TS}) as well as final state energy (E_{FS}) in reaction paths, a new BEP formula is proposed. The transition state scaling (TSS) is used to represent the new type of BEP relationship, and the equation of TSS is shown in eq11.

$$E_a = \alpha \Delta E + \beta \quad (10)$$

$$E_{TS} = \alpha E_{FS} + \beta \quad (11)$$

Where E_a and ΔE represent the activation energy and the reaction energy of the oxygen activation reaction under the Ni_n@SV-GS catalysts, respectively.

But there are few studies on the study of oxygen dissociation reaction using BEP and TSS. Therefore, the BEP and TSS relation of O₂ dissociation reactions under different Ni_n@SV-GS catalysts were calculated, as shown in Fig. 9. The detailed data were listed in Table S2.

BEP relationship can quantitatively analyze the relationship between activation energy and heat of reaction from Fig. 9(a), and the R² of the BEP relationship is 0.52, and the mean absolute error (MAE) is 0.30 eV, which is similar to the previous study (0.28 eV [50]). But the maximum y axis is 2.5 eV, which is quite large error. It is indicated that the BEP is not suitable for O₂ dissociation reaction. Fig. 9(b) showed a TSS relation for O₂ dissociation reaction on the Ni_n@SV-GS catalysts. The R² of the TSS is 0.97, which indicated that there is a good correlation between the E_{TS} and the E_{FS} , and the TSS relation is suitable for O₂ dissociation reaction. In addition, the mean absolute error (MAE) is 0.89 eV, which is larger than the value of BEP. Because the E_{TS} and E_{FS} are two orders of magnitude larger than the E_a and ΔE . In summary, the

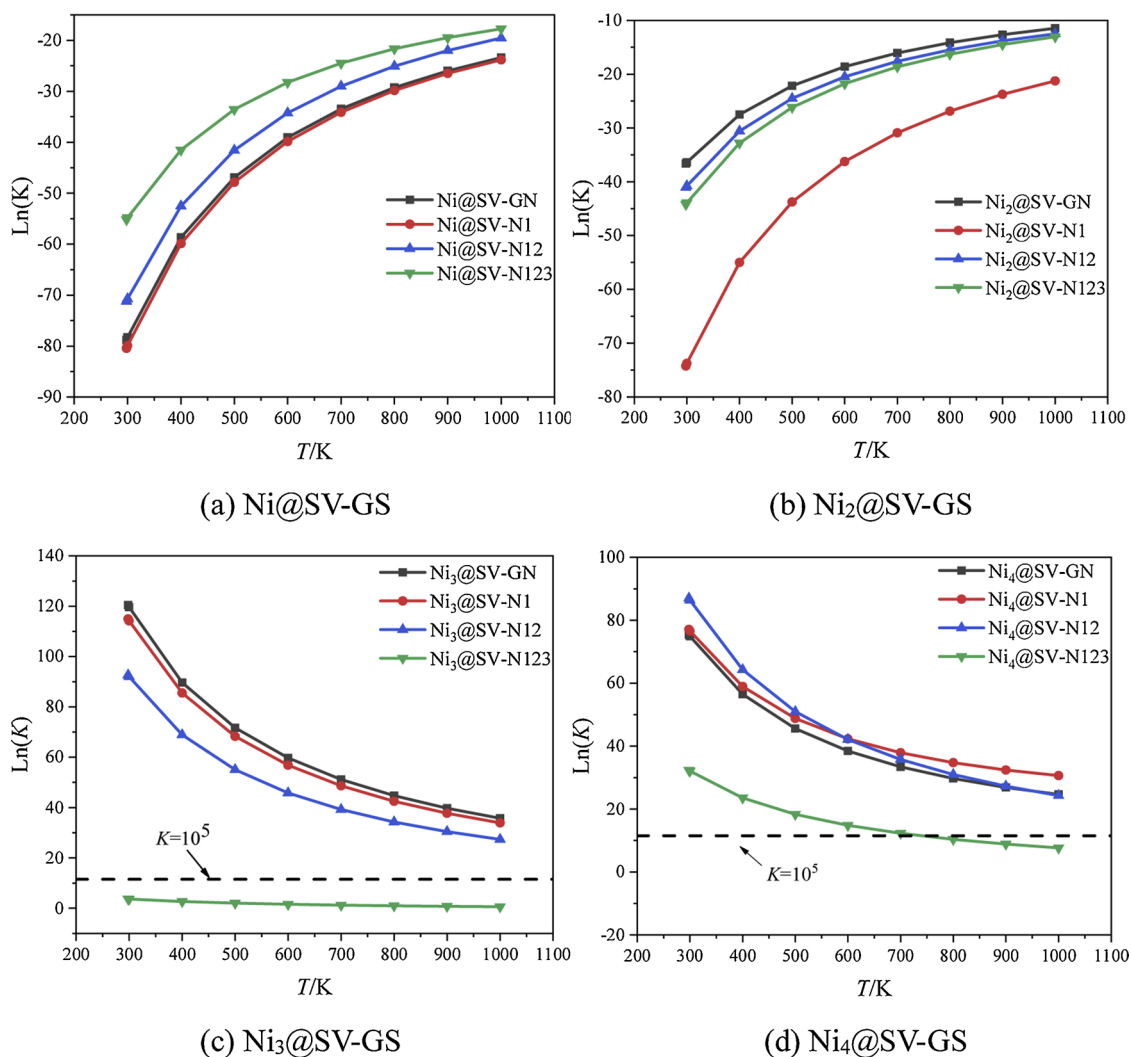


Fig. 11. The logarithm of reaction equilibrium constants of O_2 activation reaction on $Ni_n@SV-GS$ at different reaction temperatures.

TSS is suitable for O_2 dissociation reaction, and the TSS verify the accuracy of the transition state calculation.

3.5. Thermodynamic analysis

Since the activation of oxygen are affected by temperature, we will study the activation of oxygen at different temperatures. The concept of Gibbs free energy was introduced to study the effects of temperature. The calculation formula of the Gibbs free energy is as following [51]:

$$\Delta G = G_{FS} - G_{IS} = -RT \ln K \quad (12)$$

Where G_{IS} and G_{FS} are the Gibbs free energy of initial state and final state; R represents the universal gas constant ($8.61671 \times 10^{-5} \text{ eV}/(\text{mol}\cdot\text{K})$); T represents the temperature of the system; K is equilibrium constant.

To more in-depth analyze the influence of temperature variation about the oxygen activation reaction, the adsorption energy in Gibbs free energy (ΔG) and the natural logarithm of K under different temperatures (298K~1000 K) were drawn, as shown in Figs. 10 and 11. Gibbs free energy can reflect whether the reaction can proceed spontaneously and the reaction equilibrium constant can react to the extent of the reaction.

From Fig. 10, it is found that the Gibbs free adsorption energy (ΔG) of $Ni_n@SV-GS$ ($n = 1$ and 2) are all > 0 eV, and the Gibbs free adsorption energy (ΔG) of $Ni_n@SV-GS$ ($n = 3$ and 4) are all < 0 eV. It is

suggested that O_2 activation reaction can happen spontaneously when $n = 3$ and 4 and O_2 activation reaction can't happen spontaneously when $n = 1$ and 2 . From Fig. 11, it can be found that the equilibrium constants (K) of O_2 activation reaction on $Ni_n@SV-GS$ ($n = 3$ and 4) gradually decrease with the temperature increasing, which indicated that increasing the reaction temperature can promote the O_2 activation reaction. In addition, if the equilibrium constants (K) are all $> 10^5$, it is indicated that this reaction is a completely irreversible reaction.

Based on the adsorption configuration and reaction energy barrier, the previous section is found that $Ni_2@SV-N12$, $Ni_2@SV-N123$, $Ni_3@SV-N123$ and $Ni_4@SV-N123$ may become potential catalysts for oxygen activation. According to Gibbs free adsorption energy (ΔG) and equilibrium constants (K) in Figs. 10 and 11, it can be found that only the $Ni_4@SV-N123$ with the temperature at 298.15K~750 K, the ΔG is < 0 eV and the K is $> 10^5$. It is suggested that activation of O_2 on $Ni_4@SV-N123$ is a completely irreversible reaction in the 298.15K~750 K temperature range. So $Ni_4@SV-N123$ may be a promising candidate in the selection of catalysts for O_2 activation.

Next, the temperature effect on the geometry of $O_2/Ni_4@SV-N123$ will be considered by thermodynamic analysis. Therefore, we will study the activation of oxygen at different temperatures through thermodynamic analysis. The concept of Gibbs free energy was introduced to study the temperature effects. The calculation formula of the Gibbs free energy is as following:

$$\Delta G = G_{tot} - G_{Ni_n@SV-GS} - G_{O_2} \quad (13)$$

Where G_{tot} , $G_{\text{Ni}_n@SV-GS}$ and G_{O_2} represent the Gibbs free energy of the total adsorption system, the Ni cluster catalysts and the oxygen molecule.

To more in-depth analyze the influence of temperature variation about the geometry of oxygen on the $\text{Ni}_4@SV\text{-N123}$, the adsorption energy in Gibbs free energy (ΔG) under different temperatures (298K~1000 K) were drawn, as shown in Fig. S3. From Fig. S3, we can find that the ΔG is all < 0 eV when the temperature is below 1000 K. It is indicated that the adsorption of O_2 on the catalyst can happen spontaneously. Thus proved that the geometry of oxygen on the $\text{Ni}_4@SV\text{-N123}$ is firm with the temperature at 298.15K~1000 K. So temperature does not affect the geometry of the adsorption, and $\text{Ni}_4@SV\text{-N123}$ may be a promising candidate in the selection of catalysts for O_2 activation.

4. Conclusion

Using the DFT, the adsorption characteristics and reaction mechanism of O_2 activation reaction on $\text{Ni}_n@SV\text{-GS}$ catalysts were systematically and comprehensively investigated. Based on the above calculations and discussions, the optimal computing structure, the adsorption energy, the electronic gains/losses, the DOS analysis and the magnetic properties analysis were calculated to analyze the support effect of $\text{Ni}_n@SV\text{-GS}$ catalysts on O_2 adsorption and activation, and the energy barrier and the thermodynamic analysis were proposed to the catalytic activation of O_2 activation reaction. Firstly, we can find that the support effect is present during the adsorption of oxygen, and the charge of Ni atom anchored on the vacancy of graphene substrate is a descriptor of the adsorption energy of O_2 . Secondly, the electron mainly transfers from the Ni clusters to the O_2 , and the graphene-based substrates hardly work in the electron transfer process. In addition, the TSS are suitable for O_2 dissociation reaction, and the TSS verify the accuracy of the transition state calculation. Furthermore, according to the energy barrier and the thermodynamic analysis of O_2 activation reaction, $\text{Ni}_4@SV\text{-N123}$ may be an ideal candidate in selection of catalysts for O_2 activation reaction. Ultimately, we expected that this research will cast insight into activation reaction mechanism of O_2 on metal nanoclusters catalysts and lay the foundation for the investigation of metal nanoclusters catalysts for the activation reaction of O_2 .

Acknowledgements

This work was supported by the Beijing Municipal Natural Science Foundation (2182066), the Natural Science Foundation of Hebei Province of China (B2018502067) and the Fundamental Research Funds for the Central Universities (JB2015RCY03 and 2017XS121). This work was carried out at LvLiang Cloud Computing Center of China, and the calculations were performed on TianHe-2.

Appendix A. Supplementary data

Supplementary material related to this article can be found, in the online version, at doi:<https://doi.org/10.1016/j.mcat.2019.110547>.

References

- [1] T. Watanabe, *Ieee Trans. Electr. Electron. Eng.* 4 (2010) 26–26.

- [2] A. Demirbas, *Energy Sources Part A Recovery Util. Environ. Eff.* 32 (2009) 36–44.
- [3] M. Winter, R.J. Brodd, *Chem. Rev.* 104 (2004) 4245–4269.
- [4] Q. Liangti, L. Yong, B. Jong-Beom, D. Liming, *ACS Nano* 4 (2010) 1321–1326.
- [5] G. Kuanping, D. Feng, X. Zhenhai, D. Michael, D. Liming, *Science* 323 (2009) 760–764.
- [6] M. Lefevre, E. Proietti, F. Jaouen, J.P. Dodelet, *Science* 324 (2009) 71–74.
- [7] Z.J. Lu, S.J. Bao, Y.T. Gou, C.J. Cai, C.C. Ji, M.W. Xu, J. Song, R. Wang, *RSC Adv.* 3 (2013) 3990–3995.
- [8] W. Yim, T. Kluner, *J. Catal.* 254 (2008) 349–354.
- [9] T. Gao, S. Xie, Y. Gao, M. Liu, Y. Chen, Y. Zhang, Z. Liu, *ACS Nano* 5 (2011) 9194–9201.
- [10] M. Liu, Y. Zhang, Y. Chen, Y. Gao, T. Gao, D. Ma, Q. Ji, Y. Zhang, C. Li, Z. Liu, *ACS Nano* 6 (2012) 10581–10589.
- [11] K.S. Novoselov, *Int. J. Mod. Phys. B* 25 (2011) 4081–4106.
- [12] W. Wu, Q. Yu, P. Peng, Z. Liu, J. Bao, S.S. Pei, *Nanotechnology* 23 (2012) 035603.
- [13] H.J. Yan, B. Xu, S.Q. Shi, C.Y. Ouyang, *J. Appl. Phys.* 112 (2012) 104316.
- [14] Y. Li, C. He, L. Zhang, *Solid State Commun.* 267 (2017) 33–38.
- [15] S. Tang, W. Wu, L. Liu, J. Gu, *Chemphyschem* 18 (2017) 101–110.
- [16] Z.Y. Gao, W.J. Yang, X.L. Ding, G. Lv, W.P. Yan, *Phys. Chem. Chem. Phys.* 20 (2018) 7333–7341.
- [17] T. Zhang, Q. Xue, M. Shan, Z. Jiao, X. Zhou, C. Ling, Z. Yan, *J. Phys. Chem. C* 116 (2012) 19918–19924.
- [18] S. Liu, S. Huang, *Carbon* 115 (2017) 11–17.
- [19] M.M. Millet, G. Algara-Siller, S. Wrabetz, A. Mazheika, F. Girgsdies, D. Teschner, F. Seitz, A. Tarasov, S.V. Levchenko, R. Schlogl, E. Frei, *J. Am. Chem. Soc.* 141 (2019) 2451–2461.
- [20] A.T. Fiedler, A.A. Fischer, *J. Biol. Inorg. Chem.* 22 (2017) 407–424.
- [21] M.A.N. Dewapriya, R. Rajapakse, Ieee, *Effects of Free Edges and Vacancy Defects on the Mechanical Properties of Graphene*, Ieee, New York, 2014.
- [22] F. Banhart, J. Kotakoski, A.V. Krashennnikov, *ACS Nano* 5 (2011) 26–41.
- [23] Z. Gao, Y. Sun, M. Li, W. Yang, X. Ding, *Appl. Surf. Sci.* 456 (2018) 351–359.
- [24] Z. Gao, X. Liu, A. Li, X. Li, X. Ding, W. Yang, *Mol. Catal.* 470 (2019) 56–66.
- [25] K. G. F. J., *Phys. Rev. B Condens. Matter* 54 (1996) 11169–11186.
- [26] G. Kresse, J. Furthmüller, *Comp. Mater. Sci.* 6 (1996) 15–50.
- [27] G. Kresse, D. Joubert, *Phys. Rev. B* 59 (1999) 1758–1775.
- [28] K. Burke, *Phys. Rev. B* 77 (1996) 3865–3868.
- [29] G. Kresse, D. Joubert, *Phys. Rev. B* 59 (1999) 1758–1775.
- [30] P. JP, B. K, E. M., *Phys. Rev. Lett.* 77 (1996) 3865–3868.
- [31] M.D. Esrafilii, F. Sharifi, L. Dinparast, *J. Mol. Graph. Model.* 77 (2017) 143–152.
- [32] S. Gholami, A. Shokuhi Rad, A. Heydarinasab, M. Ardjmand, *J. Alloys. Compd.* 686 (2016) 662–668.
- [33] X.-Y. Xu, J. Li, H. Xu, X. Xu, C. Zhao, *New J. Chem.* 40 (2016) 9361–9369.
- [34] Z. Gao, W. Yang, X. Ding, G. Lv, W. Yan, *Appl. Surf. Sci.* 436 (2018) 585–595.
- [35] J.M. Carlsson, M. Scheffler, *Phys. Rev. Lett.* 96 (2006) 046806.
- [36] M. Gao, A. Lyalin, T. Taketsugu, *J. Phys. Chem. C* 116 (2012) 9054–9062.
- [37] J. Dong, Z. Gao, W. Yang, A. Li, X. Ding, *Appl. Surf. Sci.* 480 (2019) 779–791.
- [38] W. Yang, Z. Gao, X. Ding, G. Lv, W. Yan, *Appl. Surf. Sci.* 455 (2018) 940–951.
- [39] W. Yang, Z. Gao, X. Liu, C. Ma, X. Ding, W. Yan, *Fuel* 243 (2019) 262–270.
- [40] Z. Gao, A. Li, X. Liu, C. Ma, X. Li, W. Yang, X. Ding, *Appl. Surf. Sci.* 481 (2019) 940–950.
- [41] H. Li, G. Henkelmane, *J. Phys. Chem. C* 121 (2017) 27504–27510.
- [42] H. Li, K. Shin, G. Henkelman, *J. Chem. Phys.* 149 (2018) 8.
- [43] T. Wenjie, H. Graeme, *J. Chem. Phys.* 130 (2009) 1–351.
- [44] H. Xu, W. Chu, W. Sun, C. Jiang, Z. Liu, *RSC Adv.* 6 (2016) 96545–96553.
- [45] X. Zhou, W. Chu, W. Sun, Y. Zhou, Y. Xue, *Comput. Theor. Chem.* 1120 (2017) 8–16.
- [46] D. Farmanzadeh, T. Abdollahi, *Surf. Sci.* 668 (2018) 85–92.
- [47] B. Bunnik, G. Kramer, *J. Catal.* 242 (2006) 309–318.
- [48] A. Logadottir, T.H. Rod, J.K. Nørskov, B. Hammer, S. Dahl, C.J.H. Jacobsen, *J. Catal.* 197 (2001) 229–231.
- [49] V. Pallasana, M. Neurock, *J. Catal.* 191 (2000) 301–317.
- [50] S. Wang, V. Petzold, V. Tripkovic, J. Kleis, J.G. Howalt, E. Skulason, E.M. Fernandez, B. Hvolbaek, G. Jones, A. Toftelund, H. Falsig, M. Bjorketun, F. Studt, F. Abild-Pedersen, J. Rossmeisl, J.K. Nørskov, T. Bligaard, *Phys. Chem. Chem. Phys.* 13 (2011) 20760–20765.
- [51] W. Yang, Z. Gao, X. Liu, X. Li, X. Ding, W. Yan, *Catal. Sci. Technol.* 8 (2018) 4159–4168.